



Characterization and Applications of Innovative Sn-doped TiO₂/AC and PPy-CS/Sn-doped TiO₂ Nanocomposites as Adsorbent Materials

Elham Naser^{1,2}, Ali AL-Mokaram^{1*}, Fadhela Hussein¹

1. Department of Chemistry, College of Science, Mustansiriyah University, 10052, Baghdad, Iraq

2. Ministry of Science and Technology, Baghdad, Iraq

Received: 13 January 2021, Revised: 12 March 2021, Accepted: 15 March 2021

© University of Tehran

ABSTRACT

This work explores the synthesis and characterization of two novel nanocomposites that can be used in various applications, such as aqueous solution adsorption of pollutants. The first nanocomposite consists of tin (Sn)-doped titanium dioxide (TiO₂) on activated carbon, while the other one consists of polypyrrole (PPy), chitosan (CS), and Sn-doped TiO₂. A contrast was made of their effective adsorbent materials for the removal of Cibacron Brilliant Yellow dye from aqueous solutions. Different analytical techniques such as X-ray diffraction (XRD), scanning electron microscopy (SEM), atomic force microscopy (AFM), energy dispersive X-ray analysis (EDX), and Fourier transform - infrared (FT-IR) were used to analysis the nanocomposite samples. SEM images show that the average particle diameter of PPy-CS/Sn-doped TiO₂ NC is 75 ± 3 nm, while Sn-doped TiO₂/AC particles have an average diameter of 40 ± 2 nm. The greater PPy-CS/Sn-doped TiO₂ nanocomposite particle diameter indicates that the polymers cover the Sn-doped TiO₂ nanoparticles, which leads to higher in the diameter of the particles. The adsorption efficiency of Sn-doped TiO₂/AC was higher than that of PPy-CS/Sn-doped TiO₂ sample due to its smaller particle size which resulted in a higher surface area which provides more adsorption sites. However, both samples showed remarkable adsorption capacity, where the adsorption capacity of Sn-doped TiO₂/AC and PPy-CS/Sn-doped TiO₂ were 104 and 103 mg/g, respectively.

KEYWORDS: Nanoparticles, adsorption, CBY dye, Polypyrrole, Chitosan.

INTRODUCTION

Water pollution is a serious issue that motivated researchers to develop highly efficient and economical methods to remove these pollutants. Several methods have been investigated such as ion exchange, membranes, extraction, precipitation, and adsorption (Kalash et al., 2020; Kalash et al., 2019 & Ali et al., 2021). Adsorption is one of the wide used methods due to its high efficient and ease of operation as well as its low cost (Kalash et al., 2020). Different materials have been investigated as adsorbent such as activated carbon, agriculture waste, nanomaterials, and nanocomposite to remove different types of pollutants such as heavy metals and dyes (Alalwan et al., 2020; Kadhom et al., 2020 & Rovani et al., 2014).

High attention has been paid for synthesis of nanocomposites (NPs) due to their remarkable mechanical, physical, and chemical properties. Titanium dioxides (TiO₂) has high attractive adsorption properties which attracted researchers to use it as an adsorbent material

* Corresponding Author, Email: ali75@uomustansiriyah.edu.iq

(Alalwan et al., 2020). In addition, it has some other remarkable properties such as its nontoxicity, poor solubility, chemical stability, and high refractive index. Doping metal oxide nanoparticles (NPs) with other materials to enhance some properties such as adsorption is also under the focus of the researchers due to its important application in water and wastewater treatment. Tin (Sn) NPs have been reported to be a good adsorbent material (Nilchi et al., 2013) and Tin-sulfide (SnS) was used for doping TiO₂ on activated carbon (AC) which is usually used due to its high physical adsorption properties resulted from its high surface area (Ghaedi et al., 2013 & Roosta et al., 2014).

Synthesis of polymeric features with nano-metal oxides in a nanocomposite structure has been attracted a great attention due to their several applications in different fields such as adsorption, water treatment, biomedicine, electronic devices, sensors, and catalysis (AL-Mokaram et al., 2016). Adding polypyrrole (PPy) polymer to the nanostructures to form NC attracts high attention lately. This is due to the remarkable microstructure, electro-optical, and physiochemical properties of these NCs and the wide range of their potential applications in different fields such as a battery cathode as well as in the construction of nanoscopic assemblies in sensors and microelectronics (Mahmoudian et al., 2011). In addition, PPy was also reported to be a good adsorbent material (Kim, 2011). Synthesis of the composite in the nanoscale leads to an increasing in its total surface area which is desirable for adsorption purpose (Maddodi et al., 2020).

The deacetylated chitin derivative chitosan (CS) is a beneficial and important bioactive polymer which is an abundant material that is used for adsorption (Salih et al., 2019). As shown in Figure 1, CS has many amino groups in its structure which make it difficult for electro-spun into a fibrous structure (Oliveira et al., 2020). In addition, due to its many other important properties such as biodegradability, abundance, natural origin, and reactivity, it has wide applications including medical, food processing, agricultural, nutritional enhancement, waste and wastewater treatment, and cosmetics (Oliveira et al., 2020 & Salih et al., 2020).

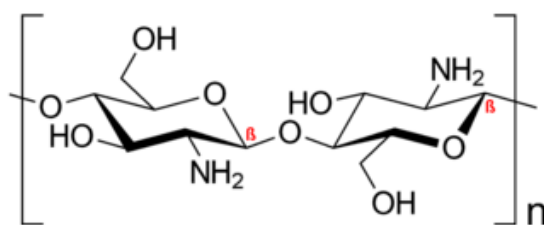


Figure 1. Chitosan Structure

Thus, this work investigates the synthesis of two novel NCs, Sn-doped TiO₂ on AC and PPy-CS/Sn-doped TiO₂ NCs and comparing their efficient as adsorbent materials to remove cybacron brilliant yellow (CBY) dye from aqueous solutions.

MATERIAL AND METHODS

Sn-doped TiO₂ /AC was prepared by sol-gel method. Titanium (IV) isopropoxide (TTIP) 99.9% supplied by Sigma-Aldrich was used as a titanium source, while ethanol and acetyl acetone were used as solvent and stabilizing agents, respectively. The mixing protocol of the composite summarized as follows:

TTIP (2.8 mol.) was mixed with ethanol and nitric acid to adjust the pH and then a small quantity of acetyl acetone was used as a peptization agent. The solution was modified by adding of 4 ml of Tin-tetra chloride (supplied by Sigma-Aldrich) solution, and created a reaction of

hydrolysis and condensation, then resulting in a transparent gel. AC (Sigma-Aldrich) which had activated by nitric acid for 24h before using was added. The reaction keeps on for an hour. This gel was dried at 100 °C, then calcinated for 120 minutes at 500 °C. Through the use of ethanol, a white powder was generated and ultrasonically cleaned for 90 minutes. The last stage was to dry it at 100 °C in an oven to get Sn-doped TiO₂ /AC in its final.

In a typical procedure 0.05 gm of Sn-doped TiO₂ NPs which was synthesized according to the previous procedure was dispersed under stirring into 20 ml of CS (0.5 mg/ml) dissolved in acetic acid at room temperature to obtain viscous of CS with uniformly dispersed Sn-doped TiO₂. In parallel, at a concentration of 0.1% of PPy was synthesized with various oxidants of p-Toluene sulfonic acid (P-TS, 0.03 M) and FeCl₃ · 6H₂O (0.5 M). In the solution of CS, Sn-doped TiO₂ NPs, and the PPy solution was sonicated for 30 minutes to allow the dispersion of pyrrole. A black greenish solution was obtained and dried at 70 °C for 24h to obtain a black powder of NC.

Sn-doped TiO₂/AC and PPy-CS/Sn-doped TiO₂ NCs were characterized using different analytical techniques. Scanning electron microscope (SEM, FEI Quanta 200) was used to investigate the surface morphology of the samples and their particle diameters. X-ray diffraction (XRD, Shimadzu 7000, Japan) was used to study the structural properties of the obtained samples. The XRD diffractograms were obtained from the Rigaku Ultima IV diffractometer (Tokyo, Japan) with Cu K α radiation of $\lambda = 1.5406 \text{ \AA}$, 40 kV, at 40 mA, using a silicon strip detector. The measurements were performed in 2 theta configurations with the scan range from 20–60 degree, with a scanning speed rate of 5 min⁻¹ and a step of 0.02.

The element analysis of the prepared samples was examined using energy dispersive X-ray spectroscopy (EDX, FEI Quanta 200). ATR-FTIR analysis was carried out using Fourier transform infrared spectroscopy (FTIR, FTIR 8400 S/ Shimadzu Japan spectrophotometer) at room temperature over the frequency range of 600-4000 cm⁻¹. Atomic Force Microscopy (AFM, Angstrom Advanced AA 3000, 220 v, USA) was used to study the surface coatings. The samples were sonicated using Ultrasonic (Elmasonic, S-300H). Samples were dried and calcinated using Electric Oven and Electric Furnace at temperatures of 100 and 500 °C, respectively.

The adsorption treatment was studied using CBY dye. The structure is shown in figure (2). Initially, 87.29 mg/l stock solution of CBY dye was prepared. The calibration curve of CBY dye was determine using different dye concentrations prepared by diluting the initial solution via distilled water. The solution absorbance was measured at a maximum wavelength 428 nm using UV-VIS spectrophotometer (CARY 100 Conc.).

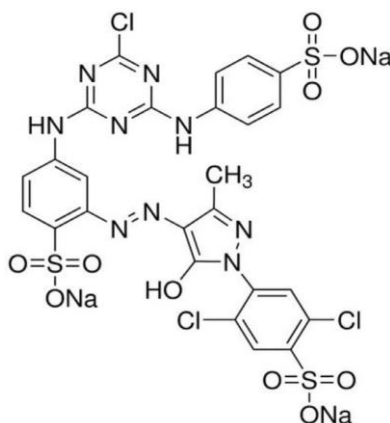


Figure 2. The chemical structure of CBY dye

The adsorption test procedure was performed by adding 0.004 gm of each sample (Sn-doped TiO₂ /AC or PPy-CS/Sn-doped TiO₂) in darkness at room temperature to 25 ml solution of CBY dye with a concentration of 87.29 ppm. The solution was stirred in darkness in a water bath (DK-2000) to let the physical adsorption of the dye molecules occurs on the adsorbent surface. In order to determine the equilibrium time, the sample was taken at the predetermined time intervals (15, 30, 45, 60, 75, 90, and 120) minutes and separated in a sigma centrifuge at 3900 rpm for 30 minutes. After wards, each dye-water sample was characterized in the spectrometer. After determining the equilibrium time, it was used as an adsorption period to investigate the adsorption efficiency of both samples at different initial CBY concentration. The dye concentration at equilibrium (C_e) was determined by using different dye concentration at equilibrium time according to Lambert-Beer equation (eq. 1).

$$A = \epsilon \cdot b \cdot C_e \quad (1)$$

where A is the absorbance at equilibrium, b is the path length of the cell, and C_e is the concentration of the compound, and ϵ is the molar extinction coefficient, which is characteristic of a particular compound at a given wavelength. The adsorbent capacity is calculated according to eq. 2.

$$Q_e = \frac{V(C_o - C_e)}{m} \quad (2)$$

where C_o is the initial concentration, V is the volume of the solution, and m is the adsorbent sample weight.

RESULTS AND DISCUSSION

Figure 3-a shows the XRD of Sn-doped TiO₂/AC NC. The XRD reveals the presence of Sn at $2\theta=32.5$ and 54.5 which are corresponding to the reflection of (002) and (301), respectively. The XRD also reveals the dominant of anatase phase of TiO₂ which gives peaks at $2\theta = 25.25$, 37.76 , and 47.97 which are corresponding to the reflection of (101), (004), and (200), respectively (Al-Ani et al., 2016). In addition, XRD pattern shows the presence of rutile phase of TiO₂ which mainly characterized by the peaks at $2\theta=27.41$ and 36.0 which are corresponding to (110) and (101), respectively. The rutile phase usually appears after using a calcination temperature between $610-915$ °C. Thus, its appearance in the Sn-doped TiO₂/AC sample which was calcinated at 500 °C is a remarkable trend that resulted from the doping with Sn (Sun et al., 2006). Activated carbon presence is characterized by the wide weak peak at $2\theta= 24$ as well as at $2\theta= 44$. Activated carbon is usually amorphous phase but it developed a little bit better crystallinity in Sn-doped TiO₂/AC NC sample due to the calcination process. However, the noise and wideness in XRD peaks indicate the persistence of amorphous phase.

Figure 3-b shows the XRD pattern of PPy-CS/Sn-doped TiO₂ NCs sample. The XRD pattern shows the same peaks that observed in the previous sample for Sn and the two phases of TiO₂. In addition, it shows chitosan peaks at $2\theta=15.4$, 15.9 , 19.0 , and 21.0 as well as some weak peaks at 2θ from 15 to 35 which are assigned to PPy.

These polymer peaks have high noise indicating that CS and PPy are more amorphous, where polymers do not develop high crystallinity even after calcination at high temperatures (Chen et al., 2016). In addition, the interaction between Ti and N atoms in the pyrrole during the polymerization process resulted in amorphous phase (Boota et al., 2016).

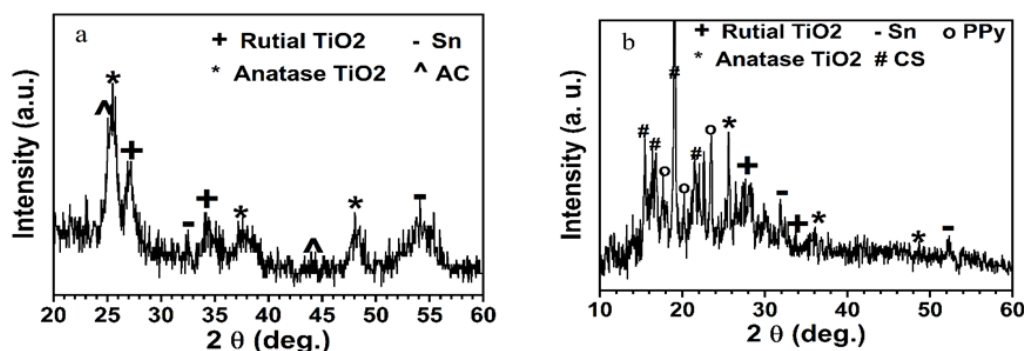


Figure 3. XRD of (a) Sn-doped TiO_2/AC and (b) PPy-CS/Sn-doped TiO_2 NCs

Figure 4-(a) and (b) shows the SEM images of Sn-doped TiO_2/AC and PPy-CS/Sn-doped TiO_2 NCs, respectively. The spherical form of particles in both samples indicates that element Sn was homogeneously dispersed in the lattice of TiO_2 . In addition, the PPy-CS/Sn-doped TiO_2 NC particles seem more organized than Sn-doped TiO_2/AC sample which indicates that both polymers (PPy and CS) cover only the surface of TiO_2 without further incorporating inside the layers of TiO_2 . SEM images was used to determine the particle diameter of each samples considering at least 100 particles from each sample as in the examples shown in figure 5-a and b. SEM images show that the average particle diameter of PPy-CS/Sn-doped TiO_2 NC is 75 ± 3 nm, while Sn-doped TiO_2/AC particles have an average diameter of 40 ± 2 nm. The bigger diameter of PPy-CS/Sn-doped TiO_2 NC particles indicates that the polymers covers the nanoparticles of Sn-doped TiO_2 which leads to increasing the particles' diameters.

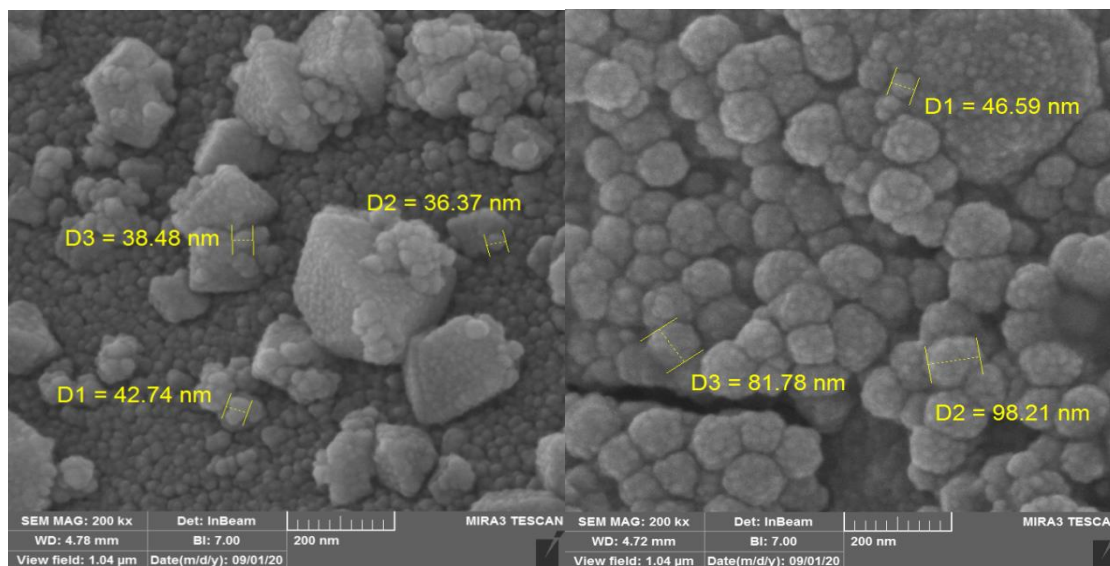


Figure 4. SEM images of (a) Sn-doped TiO_2/AC and (b) PPy-CS/Sn-doped TiO_2 NCs

The surface topography of the two samples were also investigated by AFM (Figure 5) which provides two and three dimensional (2D and 3D) images in addition to the grain size distribution. The 3D images of both samples show that each sample has bumpy shape with large number of valleys. These structures create rough surfaces which enhance the adsorption ability of both samples. The 2D images shows quasi-uniform stacked particles. The statistical analyses obtained from AFM are summarized in table 2. From table 1 data it can be noticed that Sn-doped TiO_2/AC sample has a lower grain size than PPy-CS/Sn-doped TiO_2 NCs

sample, which leads to a higher surface area for Sn-doped TiO₂/AC sample. On the other hand, PPy-CS/Sn-doped TiO₂ NCs surface has higher roughness than that of Sn-doped TiO₂/AC sample which enhances the adsorption ability of PPy-CS/Sn-doped TiO₂ sample.

Table 1. The statistical results of AFM analysis

No.	Parameter	Sn-doped TiO ₂ /AC	PPy-CS/Sn-doped TiO ₂ NCs
1	Average Roughness (nm)	4.33	14.6
2	Root Mean Square (nm)	5	17
3	Surface Skewness	0.000775	0.00632
4	Surface Kurtosis	1.8	1.91
5	Average Grain Size	67.77	79.05

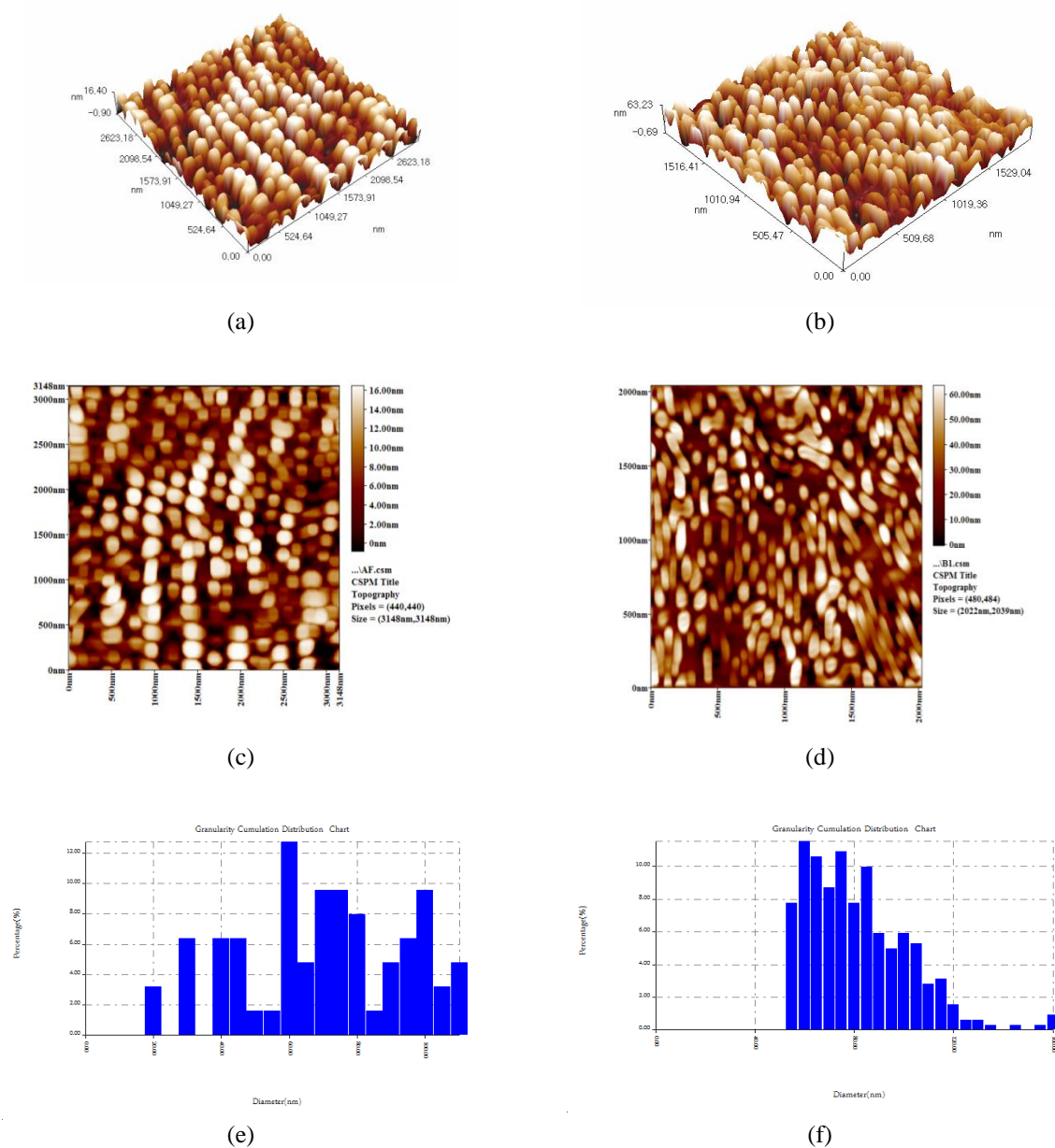


Fig 5. AFM images of (a) 3-D image of Sn-doped TiO₂/AC, (b) 3-D image of PPy-CS/Sn-doped TiO₂ NCs (c) 2-D image of Sn-doped TiO₂/AC, (d) 2-D image of PPy-CS/Sn-doped TiO₂ (e) granulometry distribution of Sn-doped TiO₂/AC, and (f) granulometry distribution of PPy-CS/Sn-doped TiO₂.

Figure 6-a shows the FTIR spectrum of Sn-doped TiO₂/AC. The band on 615 cm⁻¹ corresponds to Sn-O, while the bands at 636 and 659 cm⁻¹ are associated to Ti-O and Ti-O-Ti, respectively (Chen et al., 2015). The band observed at 1539 cm⁻¹ is assigned to the adsorbed OH group on activated carbon (Guo et al., 2007). The adsorption bands at 1050 and 1080 are assigned to C-O stretching bands. The peaks appearing at 2899 to 2922 cm⁻¹ are assigned to symmetrical and asymmetrical stretching vibration of CH₂, respectively (Song et al., 2013). Finally the bands appearing at 3700 and 3695 cm⁻¹ suggests the presence of adsorbed hydroxyl (OH) groups (Alalwan & Alminshid 2020).

The FTIR spectrum of PPy-CS/Sn-doped TiO₂ NC is shown in Figure 6-(b and c). In Fig. 6-b the adsorption band at 3389 cm⁻¹ are assigned to OH surface group, while the adsorption bands at 2922 and 2899 cm⁻¹ are assigned to C-H asymmetric and symmetric stretching vibrations, respectively (Song et al., 2013).

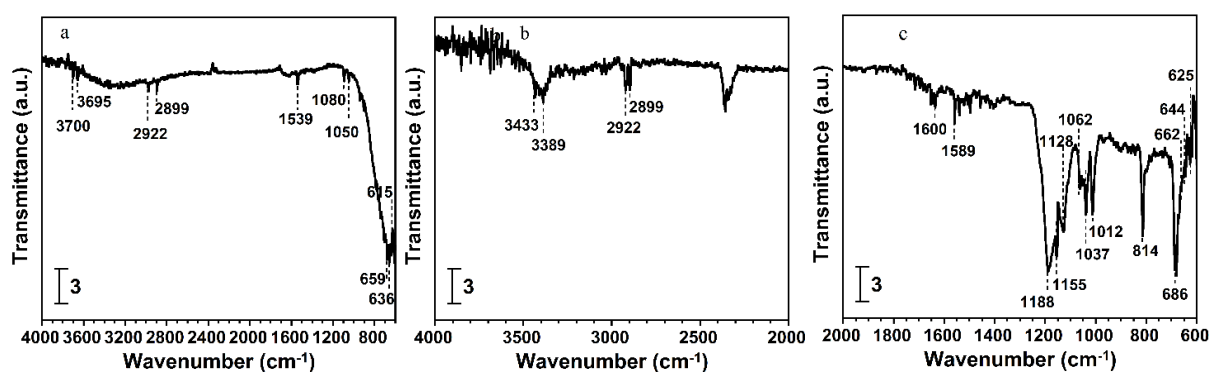


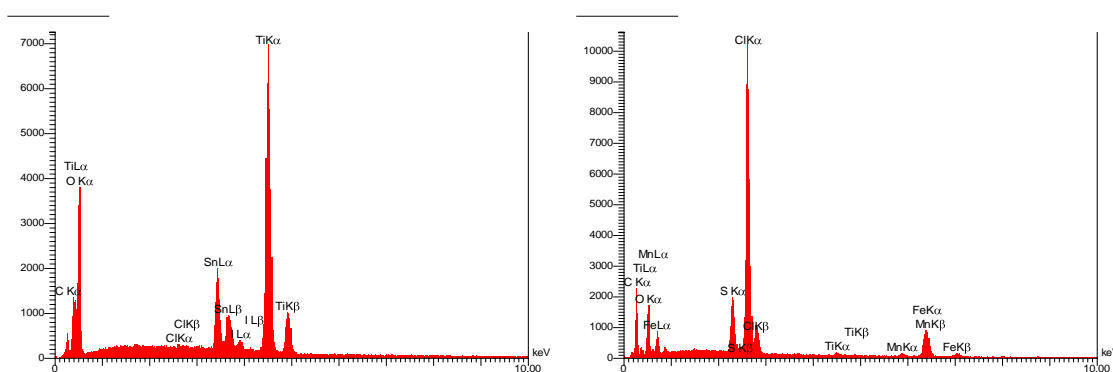
Figure 6. FTIR Spectrum of (a) Sn-doped TiO₂/AC from 600-4000 cm⁻¹ (b) PPy-CS/Sn-doped TiO₂ from 2000-4000 cm⁻¹ and (c) PPy-CS/Sn-doped TiO₂ from 600-2000 cm⁻¹.

Fig. 6-c shows the FTIR spectrum in the range from 600 to 2000 cm⁻¹. The IR spectrum shows some shifting in the Ti-O, Ti-O-Ti, and Sn-O vibrational bands. Specifically, the vibration bands at 615, 636 and 659 cm⁻¹ which are associated to Sn-O, Ti-O, and Ti-O-Ti, respectively, were shifted to 625, 644, and 662 cm⁻¹, respectively. This shifting in the wavenumbers indicates that there is an interaction between polymer backbone and Sn-doped TiO₂ nanoparticles (Mahmoudian et al., 2011). The peaks at 1012 and 1037 cm⁻¹ are attributed to the Ti-O-C (Dahham et al., 2018). The bands at 686 and 814 cm⁻¹ are due to C-H stretching in the pyrrole ring (Renjith et al., 2013). The band at 1062 is assigned to C-O stretching in primary alcohol (Chaudhuri et al., 1999), while the peaks at 1128 and 1188 cm⁻¹ are assigned to C-N bands in the pyrrole ring. The peaks observed in the range of (1400-1600) cm⁻¹ can be attributed to the fundamental vibration of pyrrole ring. The peak at 1600 cm⁻¹ corresponds to the C=C stretching vibration (Zhang et al., 2004). The FTIR was used to assess the functional groups present in the chitosan. A strong band in the region 3433 cm⁻¹ corresponds to N-H stretching band as well as at 1589 cm⁻¹ due to the N-H bending in primary amine. Finally, the band at 1155 corresponds to C-O-C bridge in chitosan (Muzzarelli et al., 2007 & Mekahlia et al., 2009).

EDX analysis was performed for both samples to identify the elements presented in each sample and their weight and atomic percentages. EDX results are shown in figure 7 and table 2. The results show that the main elements in Sn-doped TiO₂/AC samples are titanium (Ti), oxygen (O), tin (Sn), and carbon (C), while for PPy-CS/Sn-doped TiO₂ the main element is C which is main element of polymers.

Table 2. EDX analysis results of NCs samples

NCs Sample	Elements	W%	A%
Sn-doped TiO ₂ /AC	C	2.30	5.03
	O	41.68	68.26
	Cl	1.64	1.21
	Ti	41.44	22.67
	Sn	11.38	2.51
	I	1.55	0.32
PPy-CS/Sn-doped TiO ₂ NC	C	34.74	55.15
	O	16.14	19.23
	S	6.27	3.73
	Cl	36.92	19.85
	Ti	0.20	0.08
	Mn	0.18	0.06
	Fe	5.56	1.90

**Figure 7.** EDX analysis of (a) Sn-doped TiO₂/AC and (b) PPy-CS/Sn-doped TiO₂ NCs

The adsorption efficiency of both samples was investigated by applying each sample as adsorbent to remove the CBY dye from aqueous solution. First, the equilibrium time required for the adsorption process was determined by a series of experiments using different adsorption periods as shown in figure 8-a. Increasing the contact time up to 90 minutes was found to be useful to increase the removal efficiency. Increasing the time allows dye molecules to reach the active adsorption sites on the adsorbent surface and bulk which enhances the total removal efficiency. No more improvement in the removal efficiency was observed after the 90 minutes for both samples which indicates that both samples reached the equilibrium stage. The removal efficiency of Sn-doped TiO₂/AC sample was higher than that of PPy-CS/Sn-doped TiO₂. This is probably due to the higher surface area of Sn-doped TiO₂/AC sample resulted from its lower particle size which is measured by SEM analysis. Thus, the AC performance as adsorbent material seems to be better than PPy and CS polymers due to the availability of more adsorption sites on the AC resulted from its high surface area.

To confirm these findings, the removal efficiency of both samples was investigated versus different initial concentrations of CBY for 90 minutes as shown in figure 8-b. Increasing the initial concentration from 5 to 60 mg/L decreases the removal efficiency of Sn-doped TiO₂/AC sample from 72% to 62%, while it dropped the removal efficiency of PPy-CS/Sn-doped TiO₂ sample from 68% to 44%. This dropping in the removal efficiency of both samples with increasing the initial concentration is due to an increase in the adsorbate molecules which require more active adsorption sites. However, the higher dropping in PPy-CS/Sn-doped TiO₂ sample's efficiency is due to its lower number of active adsorption sites. This conclusion was

confirmed by comparing the adsorption capacity of both samples with different initial concentration as shown in figure 8-c. The adsorption capacity of both samples increases with increasing the initial concentration which can be attributed to increasing the differences between the CBY molecule numbers in the aqueous solution and the amount of active adsorption sites on the adsorbent materials which represents the driving force for CBY dye adsorption. Thus, increasing the initial concentration would enhance the CBY amount adsorbed by activate adsorbent sites but would lower the removal percentage (Maddodi et al., 2020).

From figure 8-c, it can be noticed that although there is an obvious difference in the removal percentages of the two samples, the adsorption capacity of both samples is very close. This confirm our conclusion that the lower removal efficiency of PPy-CS/Sn-doped TiO₂ sample is due to its lower available adsorption sites which leads to low removal percentage but high adsorption capacity. However, the adsorption capacity of both samples is higher than a lot of other adsorbent materials suggested for dyes removal such as modified zeolite, Fibrous peat, Canola stalk, untreated clay, and Humic which falls between 2.29 – 47.30 (Rovani et al 2014).

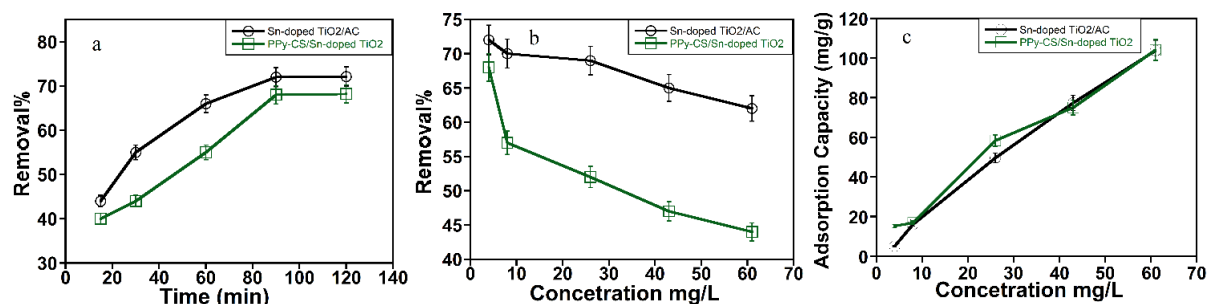


Figure 8. Using of 0.004 g of each sample to investigate (a) Impact of time on the removal efficiency using a concentration of 4 mg/L of CBY dye, (b) Impact of Increasing initial CBY concentration on the removal efficiency using 90 min as adsorption period, and (c) Impact of increasing initial CBY concentration on the adsorption capacity using 90 min as adsorption period.

CONCLUSION

Sn-doped TiO₂/AC and PPy-CS/Sn-doped TiO₂ NCs were synthesized, characterized, and applied as novel adsorbent materials to remove CBY dye from aqueous solutions. Their characterization by XRD shows the presence of both anatase and rutile phases of TiO₂ in both samples which were calcinated at 500 °C. The fact that rutile phase is formed only after calcination the sample at a temperature higher than 610 °C indicates that doping TiO₂ with Sn lowered the calcination temperature required to form the rutile phase. SEM images reveal the homogeneous shapes of both samples' particles with a spherical shape. The diameter measurements from SEM images show that the average particle diameter of PPy-CS/Sn-doped TiO₂ NC is 75 ± 3 nm, while Sn-doped TiO₂/AC particles have an average diameter of 40 ± 2 nm. The bigger diameter of PPy-CS/Sn-doped TiO₂ NC particles indicates that the polymers covers the nanoparticles of Sn-doped TiO₂ NPs which leads to increasing the particles' diameters. AFM analysis shows that PPy-CS/Sn-doped TiO₂ surface is rougher than Sn-doped TiO₂/AC which enhances its adsorption ability. FT-IR spectra of PPy-CS/Sn-doped TiO₂ NC shows some shifting in band wavenumbers of Ti-O, Ti-O₂-which suggests that polymers incorporate in the Sn-doped TiO₂ backbone. The adsorption efficiency of Sn-doped TiO₂/AC was higher than that of PPy-CS/Sn-doped TiO₂ sample due to its smaller particle

size which resulted in higher surface area that provides more adsorption sites. However, both samples showed remarkable adsorption capacity, where the adsorption capacity of Sn-doped TiO₂/AC and PPy-CS/Sn-doped TiO₂ were 104 and 103 mg/g, respectively. Increasing the adsorption capacity was observed with increasing the initial CBY concentration due to increasing the differences between the CBY molecule numbers in the aqueous solution and that adsorbed on the active adsorption sites on the adsorbent surface which represents the driving force for CBY dye adsorption.

ACKNOWLEDGEMENTS

This work is part of MSc thesis. The authors would like to thank Mustansiriyah University, College of Science- Department of Chemistry for their scientific support in this research.

GRANT SUPPORT DETAILS

The present research did not receive any financial support.

CONFLICT OF INTEREST

The authors declare that there is not any conflict of interests regarding the publication of this manuscript. In addition, the ethical issues, including plagiarism, informed consent, misconduct, data fabrication and/ or falsification, double publication and/or submission, and redundancy has been completely observed by the authors.

LIFE SCIENCE REPORTING

No life science threat was practiced in this research.

REFERENCE

- Alalwan, H. A., Abbas, M. N. and Alminshid, A. H. (2020). Uptake of cyanide compounds from aqueous solutions by lemon peel with utilising the residue absorbent as rodenticide. *Indian Chemical Engineer*, 62(1), 40-51.
- Alalwan, H. and Alminshid, A. (2020). An in-situ DRIFTS study of acetone adsorption mechanism on TiO₂ nanoparticles. *Spectrochimica Acta Part A: Molecular and Biomolecular Spectroscopy*, 229, 117990.
- AL-Ani R. R., Abdul Amir Y. K., and Hussein F. M. (2016). The Influence of Addition of CdS on the Properties of TiO₂ Nanoparticle Prepared by Sol-Gel Method.. *American Journal of Chemistry*. 6(2): 36-46.
- Ali, G. A. A., Ibrahim, S. A. and Abbas, M. N. (2021). Catalytic adsorptive of nickel metal from Iraqi crude oil using non-conventional catalysts. *Innovative Infrastructure Solutions*, 6(1), 1-9.
- AL-Mokaram, A. M. A. A., Yahya, R., Abdi, M. M. and Mahmud, H. N. M. E. (2016). One-step electrochemical deposition of Polypyrrole–Chitosan–Iron oxide nanocomposite films for non-enzymatic glucose biosensor. *Materials Letters*, 183, 90-93.
- Boota, M., Anasori, B., Voigt, C., Zhao, M. Q., Barsoum, M. W. and Gogotsi, Y. (2016). Pseudocapacitive electrodes produced by oxidant-free polymerization of pyrrole between the layers of 2D titanium carbide (MXene). *Advanced Materials*, 28(7), 1517-1522.

- Chaudhuri, P., Hess, M., Weyhermüller, T. and Wieghardt, K. (1999). Aerobic oxidation of primary alcohols by a new mononuclear CuII-radical catalyst. *Angewandte Chemie International Edition*, 38(8), 1095-1098.
- Chen, J., Feng, J. and Yan, W. (2015). Facile synthesis of a polythiophene/TiO₂ particle composite in aqueous medium and its adsorption performance for Pb (ii). *RSC advances*, 5(106), 86945-86953.
- Chen, J., Feng, J. and Yan, W. (2016). Influence of metal oxides on the adsorption characteristics of PPy/metal oxides for Methylene Blue. *Journal of colloid and interface science*, 475, 26-35.
- Dahham, O. S., Hamzah, R., Bakar, M. A., Zulkepli, N. N., Ting, S. S., Omar, M. F. and Dahham, S. S. (2018). Synthesis and structural studies of an epoxidized natural rubber/titania (ENR-50/TiO₂) hybrid under mild acid conditions. *Polymer Testing*, 65, 10-20.
- Ghaedi, M., Karimi, F., Barazesh, B., Sahraei, R. and Daneshfar, A. (2013). Removal of Reactive Orange 12 from aqueous solutions by adsorption on tin sulfide nanoparticle loaded on activated carbon. *Journal of Industrial and Engineering Chemistry*, 19(3), 756-763.
- Guo, G. S., He, C. N., Wang, Z. H., Gu, F. B. and Han, D. M. (2007). Synthesis of titania and titanate nanomaterials and their application in environmental analytical chemistry. *Talanta*, 72(5), 1687-1692.
- Kadhom, M., Albayati, N., Alalwan, H. and Al-Furaiji, M. (2020). Removal of dyes by agricultural waste. *Sustainable Chemistry and Pharmacy*, 16, 100259.
- Kalash, K. R., Alalwan, H. A., Al-Furaiji, M. H., Alminshid, A. H., and Waisi, B. I. (2020). Isothermal and Kinetic Studies of the Adsorption Removal of Pb (II), Cu (II), and Ni (II) Ions from Aqueous Solutions using Modified Chara Sp. Algae. *Korean Chemical Engineering Research*, 58(2), 301-306.
- Kalash, K. R., Kadhom, M. A. and Al-Furaiji, M. H. (2019). Short-Cut Nitrification of Iraqi Municipal Wastewater for Nitrogen Removal in a Single Reactor. In *IOP Conference Series: Materials Science and Engineering* 518(2) 022024.
- Kalash, K., Kadhom, M. and Al-Furaiji, M. (2020). Thin film nanocomposite membranes filled with MCM-41 and SBA-15 nanoparticles for brackish water desalination via reverse osmosis. *Environmental Technology & Innovation*, 20, 101101.
- Kim, K. S. (2011). Highly selective adsorption of Hg²⁺ by a polypyrrole-reduced graphene oxide composite. *Chemical Communications*, 47, 3942-3944.
- Maddodi, S. A., Alalwan, H. A., Alminshid, A. H. and Abbas, M. N. (2020). Isotherm and computational fluid dynamics analysis of nickel ion adsorption from aqueous solution using activated carbon. *South African Journal of Chemical Engineering*, 32, 5-12.
- Mahmoudian, M. R., Basirun, W. J., Alias, Y. and Ebadi, M. (2011). Synthesis and characterization of polypyrrole/Sn-doped TiO₂ nanocomposites (NCs) as a protective pigment. *Applied Surface Science*, 257(20), 8317-8325.
- Mekahlia, S. and Bouzid, B. (2009). Chitosan-Copper (II) complex as antibacterial agent: synthesis, characterization and coordinating bond-activity correlation study. *Physics Procedia*, 2(3), 1045-1053.
- Muzzarelli, R. A., Morganti, P., Morganti, G., Palombo, P., Palombo, M., Biagini, G. and Muzzarelli, C. (2007). Chitin nanofibrils/chitosan glycolate composites as wound medicaments. *Carbohydrate Polymers*, 70(3), 274-284.
- Nilchi, A., Dehaghan, T. S. and Garmarodi, S. R. (2013). Kinetics, isotherm and thermodynamics for uranium and thorium ions adsorption from aqueous solutions by crystalline tin oxide nanoparticles. *Desalination*, 321, 67-71.
- Oliveira, D. M. L., Rezende, P. S., Barbosa, T. C., Andrade, L. N., Bani, C., Tavares, D. S. and Severino, P. (2020). Double membrane based on lidocaine-coated polymyxin-alginate nanoparticles for wound healing: In vitro characterization and in vivo tissue repair. *International Journal of Pharmaceutics*, 591, 120001.

- Renjith, R., Bhagysree, J. B., Ulahannan, R. T., Varghese, H. T. and Panicker, C. Y. (2013). FT-IR, FT-Raman and Quantum Chemical Calculations of 1-phenylpyrrole. *Oriental Journal of Chemistry*, 29(1), 321.
- Roosta, M., Ghaedi, M., Daneshfar, A. and Sahraei, R. (2014). Experimental design based response surface methodology optimization of ultrasonic assisted adsorption of safranin O by tin sulfide nanoparticle loaded on activated carbon. *Spectrochimica Acta Part A: Molecular and Biomolecular Spectroscopy*, 122, 223-231.
- Rovani, S., Fernandes, A. N., Prola, L. D., Lima, E. C., Santos, W. O. and Adebayo, M. A. (2014). Removal of Cibacron Brilliant Yellow 3G-P Dye from aqueous solutions by Brazilian peats as biosorbents. *Chemical Engineering Communications*, 201(11), 1431-1458.
- Salih, S. S., Mahdi, A., Kadhom, M. and Ghosh, T. K. (2019). Competitive adsorption of As (III) and As (V) onto chitosan/diatomaceous earth adsorbent. *Journal of Environmental Chemical Engineering*, 7(5), 103407.
- Salih, S. S., Mohammed, H. N., Abdullah, G. H., Kadhom, M. and Ghosh, T. K. (2020). Simultaneous removal of Cu (II), Cd (II), and industrial dye onto a composite chitosan biosorbent. *Journal of Polymers and the Environment*, 28(1), 354-365.
- Song, C., Yu, H., Zhang, M., Yang, Y. and Zhang, G. (2013). Physicochemical properties and antioxidant activity of chitosan from the blowfly *Chrysomya megacephala* larvae. *International journal of biological macromolecules*, 60, 347-354.
- Sun, J., Wang, X., Sun, J., Sun, R., Sun, S. and Qiao, L. (2006). Photocatalytic degradation and kinetics of Orange G using nano-sized Sn (IV)/TiO₂/AC photocatalyst. *Journal of molecular catalysis A: Chemical*, 260(1-2), 241-246.
- Zhang, X. X., Bao, M., Pan, N., Zhang, Y. X. and Jiang, J. Z. (2004). IR and Raman Vibrational Assignments for Metal-free Phthalocyanine from Density Functional B3LYP/6-31G (d) Method. *Chinese Journal of Chemistry*, 22(4), 325-332.

